Applied and Environmental Microbiology

Tuning the Specificity of the Recombinant Multicomponent Toluene *o*-Xylene Monooxygenase from Pseudomonas sp. Strain OX1 for the Biosynthesis of Tyrosol from 2-Phenylethanol

Eugenio Notomista, Roberta Scognamiglio, Luca Troncone, Giuliana Donadio, Alessandro Pezzella, Alberto Di Donato and Viviana Izzo

Appl. Environ. Microbiol. **2011, 77(15):5428. DOI: 10.1128/AEM.00461-11.**
Published Ahead of Print 10 June 2011.

Applied and Environmental Microbiology, Aug. 2011, p. 5428–5437 Vol. 77, No. 15
0099-2240/11/$12.00 doi:10.1128/AEM.00461-11

Tuning the Specificity of the Recombinant Multicomponent Toluene *o*-Xylene Monooxygenase from *Pseudomonas* sp. Strain OX1 for the Biosynthesis of Tyrosol from 2-Phenylethanol▽†

Eugenio Notomista,[1] Roberta Scognamiglio,[1] Luca Troncone,[1] Giuliana Donadio,[1] Alessandro Pezzella,[2] Alberto Di Donato,[1] and Viviana Izzo[1]*

Dipartimento di Biologia Strutturale e Funzionale, Università di Napoli Federico II, Via Cinthia, I-80126 Naples, and CEINGE-Biotecnologie Avanzate s.c.ar.l., Naples, Italy,[1] and Dipartimento di Chimica Organica e Biochimica, Università di Napoli Federico II, Via Cinthia, 80126 Naples, Italy[2]

Received 1 March 2011/Accepted 1 June 2011

Biocatalysis is today a standard technology for the industrial production of several chemicals, and the number of biotransformation processes running on a commercial scale is constantly increasing. Among biocatalysts, bacterial multicomponent monooxygenases (BMMs), a diverse group of nonheme diiron enzymes that activate dioxygen, are of primary interest due to their ability to catalyze a variety of complex oxidations, including reactions of mono- and dihydroxylation of phenolic compounds. In recent years, both directed evolution and rational design have been successfully used to identify the molecular determinants responsible for BMM regioselectivity and to improve their activity toward natural and nonnatural substrates. Toluene *o*-xylene monooxygenase (ToMO) is a BMM isolated from *Pseudomonas* sp. strain OX1 which hydroxylates a wide spectrum of aromatic compounds. In this work we investigate the use of recombinant ToMO for the biosynthesis in recombinant cells of *Escherichia coli* strain JM109 of 4-hydroxyphenylethanol (tyrosol), an antioxidant present in olive oil, from 2-phenylethanol, a cheap and commercially available substrate. We initially found that wild-type ToMO is unable to convert 2-phenylethanol to tyrosol. This was explained by using a computational model which analyzed the interactions between ToMO active-site residues and the substrate. We found that residue F176 is the major steric hindrance for the correct positioning of the reaction intermediate leading to tyrosol production into the active site of the enzyme. Several mutants were designed and prepared, and we found that the combination of different mutations at position F176 with mutation E103G allows ToMO to convert up to 50% of 2-phenylethanol into tyrosol in 2 h.

Reactions in which organic compounds are oxygenated or hydroxylated are of great value for organic synthesis (33). However, selective oxyfunctionalization of organic substrates can be a significant problem in organic synthesis, as these reactions are often carried out with strong oxidizing agents and occur with little chemo-, regio-, and enantioselectivity (33, 50). Therefore, growing attention has been dedicated in the last years to the development of biotransformations which make use of the metabolic versatility of either purified enzymes or whole microorganisms to perform oxyfunctionalization of organic substrates of industrial interest (1, 7, 10, 21, 50). These methodologies, compared with established chemical processes, are appealing alternatives as means to obtain active aromatic compounds under mild experimental conditions and without employing toxic reagents (20, 26, 48).

Bacterial multicomponent monooxygenases (BMMs) allow the preparation of several aromatic active compounds with high regioselectivity and stereoselectivity (23, 41, 50). BMMs form a diverse group of nonheme diiron enzymes that activate dioxygen, thus facilitating oxygen atom transfer to specific organic substrates (32, 46), and perform a key metabolic function in promoting catabolic and detoxification reactions (55). These enzymes catalyze a variety of complex oxidations, including mono- and dihydroxylation of aromatic compounds (40, 55). BMMs usually consist of a 200- to 250-kDa dimeric hydroxylase component organized in a $(\alpha\beta\gamma)_2$ quaternary arrangement, a 10- to 16-kDa regulatory protein that enhances the catalytic turnover (3), and a FAD- and (2Fe-2S)-containing reductase that mediates the electron transfer from NADH to the active site of the hydroxylase (31, 38). An additional Rieske protein may be present to assist the electron transfer between the reductase and hydroxylase components. The hydroxylation chemistry takes place at a nonheme carboxylate-bridged diiron center, harbored in the active site of the hydroxylase moiety, coordinated by four glutamate and two histidine residues from a four-helix bundle (32, 35, 36, 38).

Oxygenase biocatalysts are already used in the chemical industry to obtain additives for agriculture, synthones, drugs, and plastics (7), and due to their catalytic properties, these multicomponent enzymes, either wild type (wt) or engineered, are a versatile biosynthetic tool for the preparation of different active aromatic compounds (8, 10, 11, 50).

Toluene *o*-xylene monooxygenase (ToMO) from *Pseudomo-*

* Corresponding author. Mailing address: Dipartimento di Biologia Strutturale e Funzionale, Università di Napoli Federico II, Via Cinthia, I-80126 Naples, Italy. Phone: 39-081-679207. Fax: 39-081-679313. E-mail: vizzo@unina.it.

† Supplemental material for this article may be found at http://aem.asm.org/.

▽ Published ahead of print on 10 June 2011.

nas sp. strain OX1 (4, 5, 15, 45) is a BMM that belongs to the subfamily of four-component aromatic/alkene monooxygenases (group 2 BMMs) (38). ToMO is endowed with a broad spectrum of substrate specificity and, among others, is able to oxidize *o*-, *m*-, and *p*-xylene, 2,3- and 3,4-dimethylphenol, toluene, cresols, benzene, naphthalene, and styrene (4).

The ToMO complex, encoded by the *tou* gene cluster (GenBank accession number AJ005663), is composed of six polypeptides which are organized as four components (15). ToMOF is the NADH oxidoreductase responsible for supplying electrons to the diiron cluster housed into the active site of the hydroxylase moiety. The electron transfer is mediated by the Rieske protein ToMOC. The hydroxylase, named ToMOH, consists of three polypeptides (B, E, A) organized in a quaternary structure of the type $(BEA)_2$; the active site is housed in the subunit ToMOA (45). Finally, ToMOD has been shown to be a regulatory protein, essential for efficient catalysis and devoid of any metal or cofactor (15). The ToMO multicomponent system has been thoroughly investigated to identify the molecular determinants responsible for its regioselective hydroxylation of aromatic compounds (12–14, 51, 52). Moreover, a computational model was recently developed that quantitatively predicts the effects of mutations into the active-site pocket of ToMOA, thus allowing the rational design of variants of the enzyme endowed with the desired regioselectivity (37).

The main aim of the present work has been to investigate the use of recombinant ToMO for the bioconversion of 2-phenylethanol, a cheap and commercially available substrate (22, 25), to the high-added-value compound tyrosol.

Tyrosol (17) belongs to a class of natural phenolic antioxidants commonly referred to as "nutraceuticals" (27) whose role in the prevention of diseases such as cancer and cardiovascular diseases is emerging (16, 18, 19, 56). Moreover, tyrosol is an excellent starting material for the microbial conversion to hydroxytyrosol (1, 2, 6, 21), an *ortho*-diphenol abundant in olive fruits and virgin olive oil, characterized by several attractive properties such as antibacterial activity, scavenging of free radicals, protection against oxidative DNA damage and low-density lipoprotein oxidation, prevention of platelet aggregation, and inhibition of 5- and 12-lipooxygenases (34, 39, 42, 43, 54).

Due to the inability of wt ToMO to produce tyrosol as the sole isomer from the hydroxylation of 2-phenylethanol, we developed a computational model to provide a molecular explanation for this outcome. To validate our computational model, several ToMO variants were designed and tested for their ability to transform 2-phenylethanol into tyrosol. Our results led to identification of residue F176 as a major steric hindrance for the correct positioning of the reaction intermediate leading to tyrosol production. In fact, all the mutations at position 176 allow ToMO to produce only tyrosol from 2-phenylethanol. Moreover, we found that the combination of mutations at position F176 with mutation E103G increases the k_{cat} values on 2-phenylethanol. Finally, among the E103G/F176X variants, we found that mutants E103G/F176I and E103G/F176T were the most efficient, allowing conversion of about 50% of 2-phenylethanol into tyrosol in 2 h.

The results presented in this paper confirm that a fine-tuning of ToMO regioselectivity can be achieved through a careful alteration of the shape of the active-site pocket. Moreover, our data indicate that this strategy can also help in designing ToMO mutants that efficiently hydroxylate, with high regioselectivity, any desired substituted benzene ring.

MATERIALS AND METHODS

Materials. Bacterial cultures, plasmid purifications, and transformations were performed according to Sambrook et al (44). *Escherichia coli* strain JM109 was from Novagen. Plasmid pTou was kindly supplied by Valeria Cafaro (Department of Structural and Functional Biology, University Federico II, Naples, Italy). The pGEM3Z expression vector, Wizard SV gel, and the PCR cleanup system for the elution of DNA fragments from agarose gels were obtained from Promega. Enzymes and other reagents for DNA manipulation were from New England BioLabs. The oligonucleotides were synthesized at MWG-Biotech (Ebersberg, Germany). All other chemicals were from Sigma. Tyrosol was purchased from Fluka. The expression and purification of recombinant catechol 2,3-dioxygenase (C2,3O) from *Pseudomonas* sp. OX1 are described elsewhere (53).

ToMOA mutagenesis and construction of expression vectors. Plasmids for the expression of ToMO complexes with mutated ToMOA subunits were obtained by site-directed mutagenesis of plasmid pTou, coding for the complete *tou* gene cluster, and prepared as previously described (13). Plasmid pTou was digested with restriction enzymes MluI and SalI to extract a 1,200-bp internal fragment from the *touA* open reading frame. This fragment lacked the first 36 bp and the last 138 bp of the coding sequence and coded for amino acids 14 to 451 of the ToMOA subunit. The MluI/SalI fragment was cloned into the pET22b(+) commercial vector, and the resulting plasmid was designated pET22b(+)/touA. This plasmid was used to obtain single mutants (F176I)-, (F176L)- (previously constructed as reported in reference 37), and (F176T)-ToMOA and double mutants (E103G/F176A)-, (E103G/F176I)-, (E103G/F176L)-, (E103G/F176T)-, (E103G/F176S)-, and (E103G/F176V)-ToMOA.

Mutations were introduced by a PCR-based methodology performed on the parent pET-22b(+)/touA plasmid using a QuikChange site-directed mutagenesis kit provided by Stratagene (La Jolla, CA), according to the manufacturer's protocol, and an MJ Research MiniCycler apparatus. PCR products were used to transform by heat shock *E. coli* XL1-Blue competent cells (Stratagene, La Jolla, CA), and cells were grown overnight on LB agar plates containing ampicillin (100 μg/ml). Three clones were picked from each plate, and their plasmids were isolated with a Qiaprep Spin Miniprep kit (Qiagen) and used for sequencing. The MluI/SalI fragments of the nine mutants were completely sequenced (MWG-Biotech), digested with MluI and SalI, and cloned back into the pTou plasmid previously digested with the same enzymes.

Identification of reaction products of ToMO-catalyzed hydroxylation of 2-phenylethanol. Reaction products were identified by high-pressure liquid chromatography (HPLC) and nuclear magnetic resonance (NMR). All the regioselectivity studies were performed using substrate concentrations higher than the K_m values. Under these conditions, absolute yields of products were proportional to k_{cat} values. Reaction products were identified with an HPLC system equipped with a Waters 1525 binary pump coupled to a Waters 2996 photodiode array detector. Products were separated using an Ultrasphere C_{18} reverse-phase column (4.6 by 250 mm; pore size, 80 Å), and the absorbance of the eluate was monitored at 254 nm for 2-phenylethanol and 276 nm for tyrosol. Separation was carried out at a flow rate of 1 ml/min by using a two-solvent system consisting of a 0.1% formic acid solution in water (solvent A) and a 0.1% formic acid solution in methanol (solvent B). Compounds were separated using a 3-min isocratic elution with 10% solvent B, followed by a 20-min linear gradient from 10 to 75% solvent B and an isocratic 5-min step at 98% solvent B. The retention times of 2-phenylethanol and tyrosol under these conditions were 24.2 and 16.4 min, respectively. The products were identified by comparing their HPLC retention times and UV-visible spectra with those of standard solutions. The amount of each product was determined by comparing the area of the peak with the areas obtained using known concentrations of standards.

For a more detailed identification of the reaction products, cell-free supernatants obtained after transformation of 2-phenylethanol were extracted twice with ethyl acetate added in a 1:2 ratio compared to the aqueous phase. The organic phase was recovered and dried with a Savant apparatus, and the pellet was dissolved in a solution of 10% methanol containing 0.1% formic acid. The sample was further purified on a high-pressure liquid chromatograph under the conditions described above; each peak was individually collected, concentrated, and used in the NMR analysis.

NMR analysis. Aliquots of the reaction mixture were withdrawn and fractionated by HPLC (see above). Fractions collected at elution times of 16.4, 17.7, and 19.6 min were then extracted with ethyl acetate (3 ml, three times). The combined organic layers were dried over sodium sulfate. The residues obtained were directly used for NMR analysis in deuterated methanol.

^{1}H NMR spectra were recorded at 600, 400, or 300 MHz, and ^{13}C NMR spectra were recorded at 75 MHz. ^{1}H and ^{13}C distortionless enhancement by polarization transfer heteronuclear single-quantum correlation and ^{1}H and ^{13}C heteronuclear multiple-quantum correlation (HMBC) experiments were run at 600 and 400 MHz, respectively, on instruments equipped with a 5 mm ^{1}H/broadband gradient probe with inverse geometry using standard pulse programs. The HMBC experiments used a 100-ms long-range coupling delay. Chemical shifts are reported in δ values (ppm) downfield from tetramethylsilane.

Regioisomers were distinguished on the base of the spin-coupling pattern in the aromatic region of the ^{1}H NMR spectra (see Fig. S1 in the supplemental material). Compound 1 showed only two signals featuring a doublet shape as a consequence of the *ortho*-type coupling. On this basis, the direct attribution of the symmetric *para*-substituted structure to compound 1, recognized as the 4-hydroxyphenylethanol, was allowed (see Fig. S1 in the supplemental material).

In the case of compounds 2 and 3 a more complex pattern in the aromatic region of the ^{1}H NMR spectra was present, suggesting a *meta* and an *ortho* substitution of the aromatic rings (see Fig. S2 and S3 in the supplemental material). The characterization of compounds 2 and 3 as 3-hydroxyphenylethanol and 2-hydroxyphenylethanol, respectively, resulted from the ratios of shielded and unshielded signals. Indeed, the ratio for compound 2 is 3 and is accounted with the two H atoms in *ortho* and the one H atom in *para* to the OH group (see Fig. S2 in the supplemental material). For compound 3, the ratio is 1, which is coherent with the presence of only two shielded H atoms, with only one in *ortho* and one in *para* to the OH group (see Fig. S3 in the supplemental material).

Whole-cell assays. The whole-cell assays were performed as previously described (12) using *E. coli* JM109 cells transformed with the plasmid of interest. Recombinant strains were routinely grown in Luria-Bertani medium (44) supplemented with 100 μg/ml ampicillin at 37°C to an optical density at 600 nm (OD_{600}) of ~0.6. Expression of the recombinant protein was induced with 0.1 mM isopropyl-β-D-thiogalactopyranoside at 37°C in the presence of 0.2 mM $Fe(NH_4)_2(SO_4)_2$. One hour after induction, cells were collected by centrifugation and suspended in M9 minimal medium containing 0.4% glucose, from here on indicated as M9-G (12). The hydroxylase activity of cells was measured using phenol as the substrate and monitoring the production of catechol in a continuous coupled assay with recombinant C2,3O from *Pseudomonas* sp. OX1, which cleaves the catechol ring and produces 2-hydroxymuconic semialdehyde. This can be monitored spectrophotometrically at 375 nm. The specific activity of cells on phenol was determined by their incubation at an OD_{600} of 0.1 to 0.5 in a quartz cuvette in a final volume of 600 μl of M9-G, 1 mM phenol, and saturating amounts of C2,3O (3 U). The rate of formation of catechol (ε_{375} = 29,100 M^{-1} cm^{-1}) was measured at 25°C.

Specific activity was expressed as the number of mU/OD_{600}, with one milliunit being defined as the amount of catalyst that oxidized 1 nmol of phenol per min at 25°C.

The determination of apparent kinetic parameters using 2-phenylethanol as a substrate was carried out by discontinuous assays with cells suspended in M9-G in a final volume of 3.5 ml at an OD_{600} of 0.5. Reactions were started by the addition to cell suspensions of various amounts of 2-phenylethanol dissolved in methanol. The final methanol concentration in cell suspensions was always kept below 5%.

At different times, a 1-ml aliquot was withdrawn and the reaction was stopped by the addition of 100 μl of 1 M HCl. Samples were centrifuged at 12,000 rpm for 30 min at 4°C. Soluble fractions were stored at −20°C until analysis. The amount of tyrosol produced from hydroxylation of 2-phenylethanol was estimated by the Folin-Ciocalteu reagent (47). The Folin-Ciocalteu reagent was used under the following conditions: 700 μl of soluble cell extract was added to 100 μl of M9-G and 50 μl of Folin-Ciocalteu reagent (Sigma). Samples were incubated for 10 min at 25°C. One hundred fifty microliters of saturated $NaHCO_3$ was added to each sample, which was then incubated for 2 h at 25°C. The A_{750} of each sample was recorded. To calculate the rate of formation of tyrosol, an extinction coefficient (ε_{750}) of 26,000 M^{-1} cm^{-1} was used.

Determination of kinetic parameters. Kinetic parameters were calculated with the program Prism (GraphPad Software). All the kinetic parameters were determined using whole cells as previously described (12–14, 37).

Maximum rate of hydroxylation (V_{max}) values for all mutants, using 2-phenylethanol as a substrate, were always normalized to the maximum rate measured on phenol in a parallel assay. This was done for each sample of induced cells, and for each mutant the experiment was repeated at least two or three times.

For each sample of induced cells, the level of expression of ToMO was measured as described below and used to calculate the apparent k_{cat} for phenol.

The amounts of ToMO complex were determined by densitometric scanning of Coomassie blue-stained sodium dodecyl sulfate-polyacrylamide gels containing cell extracts. Different amounts of samples of lysed cells were run on a single gel together with four different amounts of purified monooxygenases used as standards.

All ToMO mutants showed expression levels comparable to the level for the wild-type enzyme.

Modeling of substrates and intermediates into the active site of ToMOA. Reaction intermediates were docked into the active site of ToMO by using the Monte Carlo energy minimization strategy essentially as described previously (37) but with a few modifications: (i) conformational energy calculations included a hydration component calculated as described previously (29, 30) (the hydration energy of Zn^{2+} was arbitrarily assigned to iron ions), (ii) the inner shell included 30 ToMO residues surrounding the active-site cavity, and (iii) complexes with total energies of up to 4 kcal/mol higher than that of the lowest-energy complex were stored for the analysis of energy contributions. 2-Phenylethanol was docked as described above for reaction intermediates but with the following modifications: (i) no hydration component was assigned to the iron ions, and (ii) the inner shell and the outer shell were enlarged to 51 and 181 ToMO residues, respectively. The docking of phenylethanol was performed in three steps: (i) the ToMO-phenylethanol complexes were minimized with phenylethanol locked to an orientation similar to that of the reaction intermediate for the hydroxylation at the *para* position using the atom-atom distance constraints; (ii) the centroid and grid functions were used to generate eight orientations of phenylethanol inside the active-site cavity; and (iii) the eight ToMO-phenylethanol complexes were minimized without constraining the orientation of phenylethanol, except that the oxygen-iron distances were constrained to values higher than 4 Å to avoid the accumulation of complexes with the oxygen atom of phenylethanol at a bridging position between the iron ions.

The Protein Data Bank files for the initial manually generated complexes and the ZMM instruction files containing the lists of mobile residues, constraints, and parameters used during calculations are available upon request.

Other methods. Polyacrylamide gel electrophoresis was carried out using standard techniques (28, 44). Tris-glycine gels were run as 18% gels under denaturing conditions. Protein concentrations were determined colorimetrically with the Bradford reagent (9) from Sigma, using 1 to 10 μg bovine serum albumin as a standard.

RESULTS AND DISCUSSION

ToMO-catalyzed hydroxylation of 2-phenylethanol. On the basis of the similarity between 2-phenylethanol and the natural aromatic substrates of ToMO, we investigated the possibility of using this multicomponent enzyme to hydroxylate 2-phenylethanol to form tyrosol.

Cells of *E. coli* strain JM109 transformed with plasmid pBZ1260 expressing the ToMO gene cluster were grown in LB medium, and the expression of the recombinant multicomponent system was induced as described in Materials and Methods. After 1 h of induction, cells were collected by centrifugation, resuspended in M9-G at a final concentration of 6 OD_{600} units, and incubated with 5 mM 2-phenylethanol. After incubation for different times (0.5, 2, 4, and 14 h) under constant shaking, 1-ml samples were withdrawn, cells were collected by centrifugation, and the supernatants were analyzed by HPLC as described in Materials and Methods. HPLC chromatograms showed that ToMO was able to hydroxylate 2-phenylethanol. Three different peaks were evident from the chromatogram (Fig. 1); the peaks were manually collected and identified by NMR (see Materials and Methods and Fig. S1 to S3 in the supplemental material). The analysis showed that the compound eluting in peak 1 (at 16.4 min) was 4-hydroxyphenylethanol (tyrosol; from here on indicated *p*-tyrosol [10]), the compound eluting in peak 2 (at 17.7 min) was 3-hydroxyphenylethanol (from here on indicated *m*-tyrosol [10]), and the

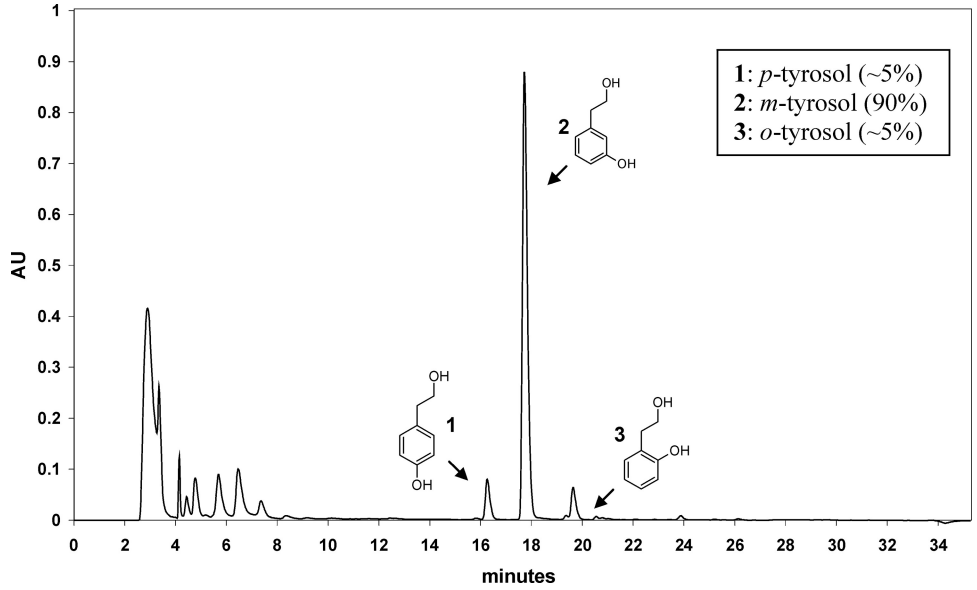

FIG. 1. Regioselectivity of the ToMO-catalyzed reaction using 2-phenylethanol as a substrate. An HPLC chromatogram was monitored at a λ of 276 nm and showed the presence of three products (compounds 1, 2, and 3) corresponding to *p*-tyrosol, *m*-tyrosol, and *o*-tyrosol, respectively. AU, absorbance units. (Inset) Relative percentages of each product.

compound eluting in peak 3 (at 19.6 min) was 2-hydroxyphenylethanol (from here on indicated *o*-tyrosol [10]). *m*-Tyrosol accounted for ca. 90% of the total yield of product, whereas *p*-tyrosol and *o*-tyrosol accounted only for ca. 5% each. It should be noted that the preferential regioselectivity of the ToMO-catalyzed reaction toward the *meta* position of 2-phenylethanol has recently been reported (10). Hence, it was evident that 2-phenylethanol can be hydroxylated by ToMO mainly to *m*-tyrosol, whereas the desired product, *p*-tyrosol, was produced in very low yields. Kinetic parameters of the hydroxylation reaction using 2-phenylethanol as a substrate were calculated in discontinuous assays using whole recombinant cells of *E. coli* strain JM109, as described in the Materials and Methods section. The K_m using this substrate is 211 ± 22 μM, and the k_{cat} value is 0.054 ± 0.016 s^{-1}.

Docking of 2-phenylethanol into active site of ToMOA. A computational strategy, based on a Monte Carlo approach, was recently developed that quantitatively predicts the effects of mutations in the active-site pocket of the hydroxylase moiety of ToMO on the regioselectivity shown by this enzyme on physiological substrates (37). Our aim has been to broaden this computational strategy and to use its predictions to tune ToMO regioselectivity and catalytic efficiency also on nonphysiological substrates.

Briefly, the computational strategy is based on a simple kinetic model which predicts the regioselectivity on aromatic substrates of ToMO and its mutants by calculating the relative stability of the orientations of different transition states generated by different enzyme-substrate complexes (37) (Fig. 2A and B). In this model the substrate binds to the active site in different orientations, generating productive and unproductive enzyme-substrate complexes (Fig. 2B). The three possible productive complexes are in equilibrium both with the unproductive complexes and with the three transition states, leading to the *o*-, *m*-, and *p*-substituted phenols (*o*C, *m*C, and *p*C, respectively, in Fig. 2B). According to this kinetic model, the regioselectivity of the enzyme depends only on the relative stability of the three different transition states. This assumption allows us to predict the relative abundance of the products by docking the putative high-energy intermediates (arenium ions in Fig. 2A) into the active site (37).

However, the kinetic model shown in Fig. 2B also suggests that the catalytic efficiency and, in particular, the apparent k_{cat} value of a ToMO mutant should depend both on the absolute stability of the transition state(s) and on the relative abundance of the productive and unproductive enzyme-substrate complexes (Fig. 2B). Thus, the model will predict an efficient ToMO-catalyzed hydroxylation of a substituted benzene like 2-phenylethanol to a desired substituted phenol, e.g., *p*-tyrosol, (i) if the high-energy intermediate corresponding to the desired phenol product fits the active site well and fits better than any other possible high-energy intermediate and (ii) if the ToMO-substrate complex in which the substrate is productively oriented for catalysis is the most abundant one.

We have previously suggested (37) that the stability of the transition state is the sum of two contributions: (i) a noncovalent contribution (noncovalent binding energy [ncBE]) depending on noncovalent interactions between the high-energy intermediate and the active-site pocket, which can be calculated by molecular mechanics techniques like Monte Carlo docking (37), and (ii) a covalent contribution depending on the bonds between the oxygen atom of the high-energy intermediate and the iron ions of the cluster, i.e., on the geometrical parameters of the diiron clusters-arenium ion complex (Fig. 2A and C), which can be calculated only by a complex quantum-mechanical treatment of the transition state. However, the Monte Carlo docking of benzene, toluene, and *o*-xylene arenium intermediates showed that the arenium ring of all the intermediates deriving from these physiological substrates adopts very similar orientations within the active-site pocket of

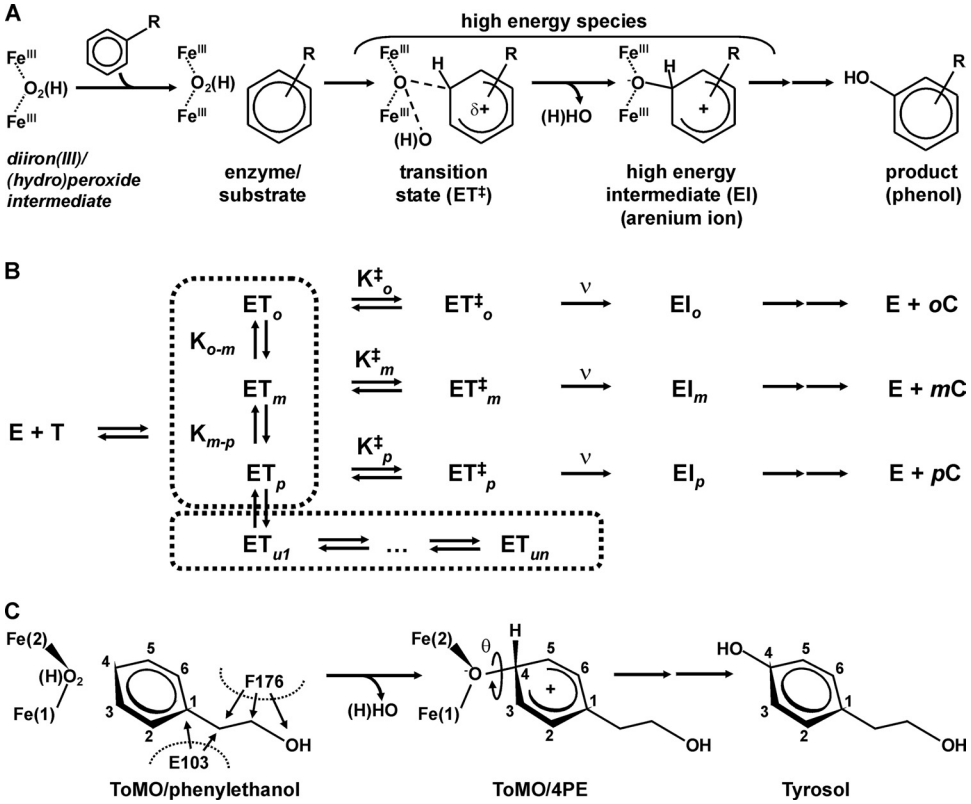

FIG. 2. Kinetic model depicting the regioselectivity of ToMO-catalyzed reactions. (A) Hypothetical enzyme-substrate intermediates during the hydroxylation of an aromatic substrate in the active site of ToMOA; (B) distribution and kinetic constants of productive and nonproductive enzyme-transition state complexes; (C) modeling of the 4-hydroxyphenylethanol intermediate in the active site of ToMOA.

wild-type ToMO (37). Therefore, these Monte Carlo energy-minimized complexes can be considered a reliable model of the optimal transition state for the aromatic hydroxylation reaction and can be used as a reference structure to analyze interactions between the ToMO active site and the high-energy intermediates deriving from nonnatural substrates of this enzyme (37).

In this study we used as a reference structure the Monte Carlo energy-minimized complex between wild-type ToMO and the high-energy intermediate for the conversion of toluene to *p*-cresol, since this reaction is similar to the desired hydroxylation of 2-phenylethanol to *p*-tyrosol.

Table 1 shows that a correlation exists between the k_{cat} values on toluene of some ToMO mutants (37) and the predicted orientation of the arenium intermediates for the toluene/*p*-cresol reaction with respect to that of our reference structure. Two geometrical parameters defining the orientation of the arenium ring with respect to the diiron cluster were used for the comparison: (i) the distance between the C-4 atom of the mutant-generated complex and the C-4 atom of the reference complex, and (ii) $\Delta\theta$, a parameter that measures the angle deviation of the plane of the arenium ring in a ToMO mutant-intermediate complex with respect to the plane of the arenium ring in the reference structure. θ, whose value in the reference structure is 103.6°, is the torsion angle Fe-2–O–C-4–C-3 (Fig. 2C). It should be noted that the choice of the C-4 atom was made on the basis of the critical importance of this position of the substrate, which is responsible for accepting the oxygen atom from the diiron cluster during the hydroxylation reaction (Fig. 2A).

It is evident from the data in Table 1 and Fig. S4 in the supplemental material that ToMO mutants characterized by C-4–C-4 distances less than 0.15 Å and $\Delta\theta$ values of about $-10°$ to $+5°$ show high k_{cat} values (similar to or greater than

TABLE 1. Geometric parameters of the complexes between ToMO and ToMO mutants and the arenium intermediate for the toluene/*p*-cresol reaction

Complex	C-4–C-4 (Å)	$\Delta\theta$ (°)	k_{cat} (s^{-1})[a]
(L100, G103)/S4M[b]	0.05	−9.0	0.67
L100/S4M	0.06	−1.2	0.56
wt/S4M	0	0	0.43
G103/S4M	0.04	−6.8	0.42
(I180, G103)/S4M	0.04	−6.5	0.34
L176/S4M	0.11	−2.1	0.32
I176/S4M	0.07	+2.0	0.28
I103/S4M	0.15	+3.8	0.22
(V103, V100)/S4M	0.2	+2.5	0.097
A100/S4M	0.05	+12.0	0.03
I103/S4M	0.23	+15.0	0.030
V107/S4M	0.40	−7.1	0.024
I107/S4M	0.49	−9.2	0.0009

[a] k_{cat} values are from reference 37.
[b] S4M, toluene/*p*-cresol.

TABLE 2. Geometric parameters and ncBEs of the complexes between ToMO and ToMO mutants and the arenium intermediates for the 4PE, 3PE, and 2PE reactions

Amino acid		Arenium ion								
		4PE			3PE			2PE		
Position 103	Position 176	C-4–C-4 (Å)	Δθ (°)	ncBE (kcal mol^{-1})	C-4–C-4 (Å)	Δθ (°)	ncBE (kcal mol^{-1})	C-4–C-4 (Å)	Δθ (°)	ncBE (kcal mol^{-1})
Glu[a]	Phe[a]	0.30	+41	−7.8	0.23	+22	−5.7	0.37	+44	−5.0
Gly[b]	Phe[b]	0.28	+41	−7.5	0.23	+24	−5.6	—[c]	—	—
Glu	Ala	0.20	−10	−11.0	0.20	+17	−9.5	—	—	—
Glu	Ile	0.13	−4	−11.0	0.31	+35	−8.9	—	—	—
Glu	Leu	0.17	−6	−11.1	0.35	+37	−7.5	—	—	—
Glu	Ser	0.15	+9	−10.9	0.22	+20	−9.3	—	—	—
Glu	Thr	0.20	−10	−11.0	0.22	+17	−9.4	—	—	—
Glu	Val	0.14	−6	−11.0	0.21	+15	−9.5	—	—	—
Gly	Ala	0.08	−14	−11.8	0.22	+22	−9.0	—	—	—
Gly	Ile	0.08	−10	−11.7	0.20	+16	−8.5	—	—	—
Gly	Leu	0.14	−5	−10.8	0.30	+38	−6.3	—	—	—
Gly	Ser	0.06	−11	−11.5	0.22	+18	−8.9	—	—	—
Gly	Thr	0.05	−11	−11.5	0.20	+30	−8.9	—	—	—
Gly	Val	0.05	−7	−11.5	0.18	+29	−8.8	—	—	—

[a] Wild-type ToMOA.
[b] (E103G)-ToMOA.
[c] —, not determined.

those for wild-type ToMO), whereas ToMO mutants characterized by C-4–C-4 distances higher than 0.2 Å and/or Δθ values >+5° show k_{cat} values significantly lower than those measured for the wild-type enzyme.

Hence, we docked into the active site of wild-type ToMO the three high-energy intermediates for the hydroxylation of 2-phenylethanol to *o*-, *m*-, and *p*-tyrosol (these intermediates are indicated 2PE, 3PE, and 4PE, respectively, from here on). As shown in Table 2, the geometries of all the high-energy intermediates showed considerable deviations from the ideal geometry, in agreement with the fact that wild-type ToMO is a bad catalyst for the 2-phenylethanol hydroxylation (k_{cat} value, 0.054 ± 0.016 s^{-1}) compared to the natural substrate toluene (k_{cat} value, 0.43 s^{-1}). The highest deviations from the ideal orientation were observed in the case of the intermediates 2PE and 4PE, and the lowest was observed for the intermediate 3PE, in agreement with the observation that wild-type ToMO produces ca. 90% *m*-tyrosol.

A close inspection of the model of the ToMO-4PE complex (Fig. 3A), i.e., the analog of the intermediate leading from 2-phenylethanol to the desired substituted phenol, e.g., *p*-tyrosol, showed that van der Waals contacts between the side chain of Phe-176 and the hydroxyethyl moiety of 4PE that are too close prevent the positioning of the arenium ring of this intermediate in an orientation similar to that of the reference structure, thus providing a geometrical explanation for the low production of *p*-tyrosol by wild-type ToMO (Fig. 3A and B). We repeated the same analysis on six ToMO mutants with smaller residues at position 176 (Ile, Leu, Val, Thr, Ser, and Ala). In this case, the docking procedure was carried out only with the high-energy intermediates 3PE and 4PE, because a preliminary analysis revealed that mutations at position 176 did not significantly change the C-4–C-4, Δθ, and ncBE values for 2PE with respect to that measured for wt ToMO (data not shown).

The data in Table 2 indicate that the geometrical parameters of most of these mutants show a better similarity of their complexes with the reference structure only in the case of the arenium ring of 4PE, the intermediate leading to *p*-tyrosol. The data show that for all mutations at position 176, the orientation of the 4PE intermediate is more similar to that of the reference model than that of wt ToMO: the C-4–C-4 distances are between 0.13 and 0.20 Å and the Δθ values are between −9° and +10°. However, these values are out of the limits defined from the data in Table 1. Moreover, a careful inspection of these complexes revealed that the side chain of Glu-103, which, in wt ToMO, is closely packed to the Phe-176 side chain, could limit the conformational freedom of the side chain of residues modeled at position 176. Therefore, we also modeled six double mutants in which all the mutations at position 176 were coupled with mutation E103G, which could, in principle, remove the hindrance of the bulky side chain at position 103. Data in Table 2 show that for all the double mutants, with the exception of ToMO mutant (E103G, F176L), the C-4–C-4 distances are less than 0.1 Å and Δθ values are less than 0°, i.e., within the limits defined from the data in Table 1 for high-k_{cat} mutants, only when docking the arenium ring of 4PE. It is also worth noting that as the orientation of the intermediate 4PE becomes more similar to that of the reference model complex, the ncBE of the intermediate becomes more negative, thus indicating a better fit between the 4PE intermediate and the active-site pocket.

Thus, on the basis of our assumption, i.e., that a correlation exists between the k_{cat} values and the predicted orientation of the arenium rings compared to that of the reference structure, we can hypothesize that all mutations at position 176, both alone and in combination with mutation E103G, selectively improve the binding of the intermediate 4PE. As a consequence, these mutants should exclusively produce *p*-tyrosol.

However, according to our kinetic model, a good positioning of the arenium intermediate, although essential, is not a sufficient condition for an efficient catalysis, given that mutations

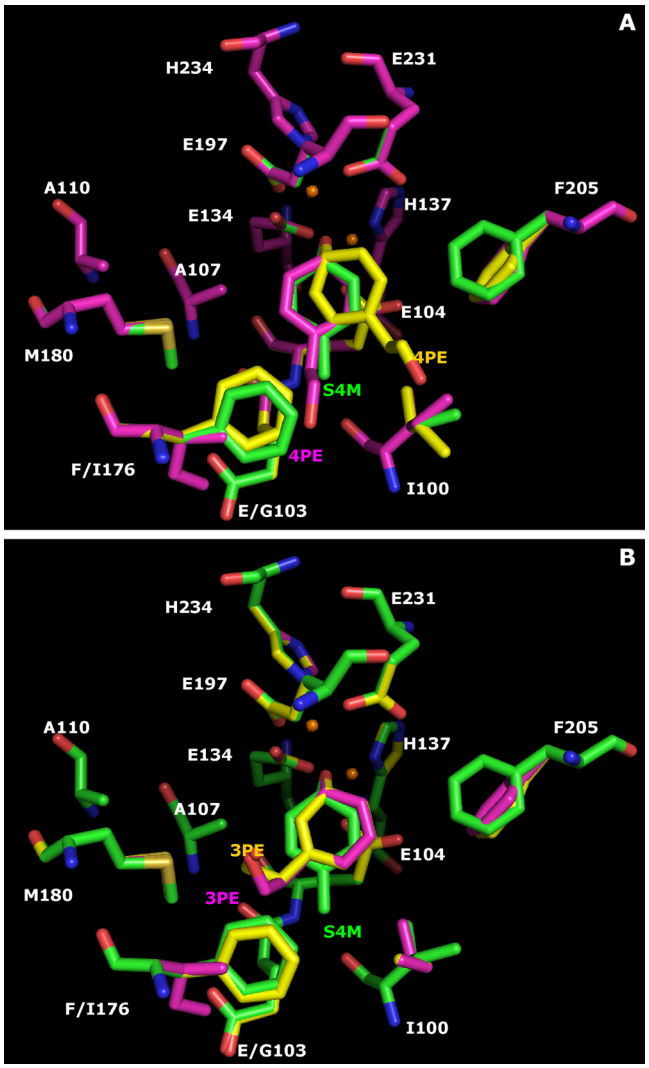

FIG. 3. Structures of the complexes between wt ToMO or ToMO mutants and the arenium intermediates for the reactions 4PE (A), 3PE (B), and toluene/*p*-cresol (S4M) (A and B). Carbon atoms are shown in green (S4M/ToMO), yellow (4PE/ToMO and 3PE/ToMO), and magenta [4PE/(E103G, F176I)-ToMO and 3PE/(E103G, F176I)-ToMO]; oxygen atoms are shown in red, and nitrogen atoms are shown in blue. Hydrogen atoms are not shown.

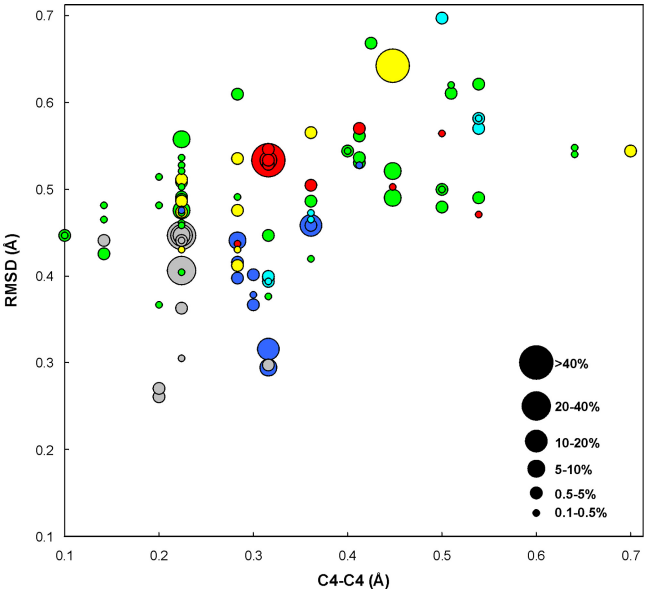

FIG. 4. Calculated relative abundance (in percent) of the ToMO–2-phenylethanol complexes as a function of the distance between the C-4 atom of the 2-phenylethanol and the C-4 atom of the reference structure and of the RMSD between the ring of 2-phenylethanol and the ring of the reference structure. Red circles, (E103G, F176A)-ToMO; gray circles, (E103G, F176I)-ToMO; cyan circles, (E103G, F176L)-ToMO; blue circles, (E103G, F176S)-ToMO; green circles, (E103G, F176T)-ToMO; yellow circles, (E103G, F176V)-ToMO.

which stabilize unproductive orientations of the substrate will reduce the apparent k_{cat} value. Therefore, even if all the double mutants bind the 4PE intermediate in a correct orientation and with similar noncovalent binding energies, different k_{cat} values could be obtained.

In order to predict which double mutant(s) is the best catalyst(s) for the production of *p*-tyrosol, it is necessary to define a strategy to predict the ratio between the abundance of productive and nonproductive enzyme-substrate complexes. Monte Carlo docking of the substrate 2-phenylethanol provides a panel of possible orientations of the substrate in the active site of the double mutants, whereas comparison of the orientations of 2-phenylethanol in the complexes and the reference structure, i.e., the complex between wild-type ToMO and the arenium intermediate for the conversion of toluene to *p*-cresol, helps to discriminate between productive and nonproductive enzyme-substrate complexes. Thus, we docked 2-phenylethanol into the active site of the double mutants; the total energies of the complexes were calculated and used to estimate their relative abundance at equilibrium. Finally, we compared the orientations of the substrate in these complexes with the orientation of the arenium intermediate in the reference structure. Figure 4 shows the abundance of the ToMO-phenylethanol complexes as a function of the distance between the C-4 atom of 2-phenylethanol and the C-4 atom of the reference structure (*x* axis) and of the root mean square deviation (RMSD) between the ring of phenylethanol and the arenium ring of the reference structure (*y* axis). It should be noted that as 2-phenylethanol is not covalently bound to the diiron cluster, in this case, the Fe-2–O–C-4–C-3 torsion angles, θ, are meaningless.

Data in Fig. 4 show that the double mutants dock 2-phenylethanol in slightly different orientations. (E103G, F176T)- and (E103G, F176I)-ToMO show high percentages of complexes with very short C-4–C-4 distances and RMSDs, respectively. This means that in this case 2-phenylethanol adopts in the active site orientations very similar to the orientation of the arenium ion of the reference structure, thus suggesting that the active sites of these mutants can properly orient the substrate for catalysis. On the contrary, only complexes with both relatively long C-4–C-4 distances and RMSDs are predicted for a mutant like (E103G, F176A)-ToMO, suggesting that in this mutant a larger rearrangement is necessary to switch from the enzyme-substrate complex to the transition state (the enzyme-arenium ion complex). The remaining three double mutants show an intermediate behavior. On the basis of our data,

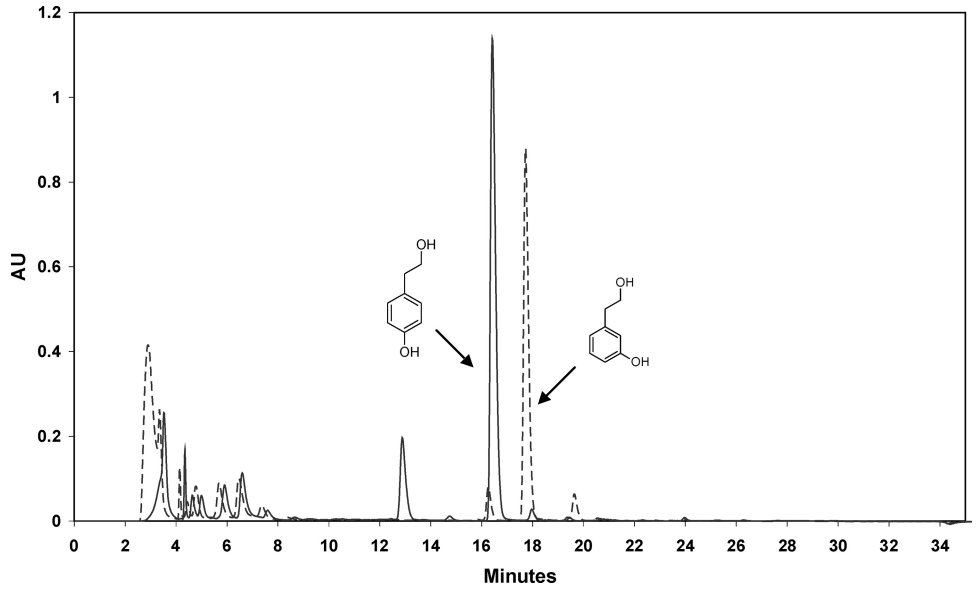

FIG. 5. Regioselectivity of ToMO/F176T-catalyzed reaction using 2-phenylethanol as a substrate (solid line). An HPLC chromatogram monitored at a λ of 276 nm shows the presence of a single product corresponding to *p*-tyrosol. The dashed-line trace is the HPLC profile monitored under the same experimental conditions using wt ToMO. Results are similar for both the F176X and E103G/F176X mutants. AU, absorbance units.

we can predict the following order of k_{cat} values: (E103G, F176T)- and (E103G, F176I)-ToMO > (E103G, F176L)-, (E103G, F176V)-, and (E103G, F176S)-ToMO > (E103G, F176A)-ToMO.

To validate our hypothesis, we prepared and characterized mutants with single mutations of ToMOA, i.e., F176I, F176L, and F176T, as well as mutants with double mutations, E103G-F176(I, L, T, A, S, V), to verify whether these changes would affect the catalytic efficiency of the enzyme on 2-phenylethanol according to our predictions.

Identification of reaction products and determination of kinetic parameters of ToMO mutant-catalyzed hydroxylation of 2-phenylethanol. Enzymatic assays on recombinant whole cells of *E. coli* strain JM109 expressing ToMOA mutants and using 2-phenylethanol as substrate were carried out as described in the Materials and Methods section. Reaction products were identified by HPLC and NMR. Our results (Fig. 5) clearly indicate that substitution of residue F176 is essential to obtain almost exclusively *p*-tyrosol from 2-phenylethanol. For all mutants with a mutation at position 176, no detectable *o*-tyrosol was observed and *m*-tyrosol yields were less than 2%. Also, double mutants produced only *p*-tyrosol, whereas ToMOA variant E103G shows the same regiospecificity as the wild-type enzyme on 2-phenylethanol (data not shown). The analysis of the kinetic parameters (Table 3) indicates that variants bearing E103G/F176X mutations have higher k_{cat} values on 2-phenylethanol than the corresponding variants with single mutations. Therefore, confirming our hypothesis, it seems that reduction of steric hindrance at position 103 (13, 37, 45) acts in a synergistic manner with mutations at position 176. Global reduction of steric hindrance inside the active site likely allows for a better fitting of 2-phenylethanol, resulting in an increase of the k_{cat} value. It should be noted, however, that the strategy of widening the active site fails to be effective when the data obtained for mutant E103G/F176A are analyzed. In this case, in fact, an excessive broadening of the active site leads to a drastic decrease in the catalytic efficiency of the enzyme, likely due to a degree of freedom of 2-phenylethanol inside the active site of this mutant that is too high.

The higher k_{cat} value measured on 2-phenylethanol is obtained with variant E103G/F176T. The Monte Carlo-minimized models show that in this double mutant the —OH group of threonine forms an H bond with the backbone oxygen atom of Ala-172, whereas the methyl group points toward the active-site cavity and makes van der Waals interactions with the hydroxyethyl group of both 2-phenylethanol and the 4PE intermediate (see Figure S5A and B in the supplemental material). Thus, the model suggests that the active site of mutant E103G/F176T allows for the appropriate orientation of both the substrate and the intermediate. In this mutant, however, van der Waals contacts between the methyl group of the threonine residue and the hydroxyl group of 2-phenylethanol involve a partial desolvation of the hydroxyl group of the sub-

TABLE 3. Apparent K_m and k_{cat} values of ToMO and ToMO mutants using 2-phenylethanol as substrate

Mutant	K_m (μM)	k_{cat} (s^{-1})
wt	211 (±22)	5.4 (±1.6) × 10^{-2}
F176I	392 (±28)	2.8 (±0.1) × 10^{-2}
F176L	276 (±52)	3.8 (±0.5) × 10^{-2}
F176T	662 (±46)	14.0 (±0.5) × 10^{-2}
E103G/F176A	404 (±25)	6.0 (±0.1) × 10^{-2}
E103G/F176I	759 (±160)	47.0 (±4.0) × 10^{-2}
E103G/F176L	362 (±44)	18.0 (±0.7) × 10^{-2}
E103G/F176T	1,045 (±66)	71.0 (±1.9) × 10^{-2}
E103G/F176S	557 (±42)	14.5 (±0.5) × 10^{-2}
E103G/F176V	435 (±52)	14.9 (±0.6) × 10^{-2}

strate (see Fig. S5B in the supplemental material), thus determining a decrease of the apparent affinity for the substrate (i.e., an increase of the K_m value; Table 3).

Thus, our experimental results are in good agreement with the computational model. First, the model identified residue F176 as the major constraint for the productive orientation of the 4PE reactive intermediate. Moreover, our model correctly predicts an increase of the k_{cat} value on 2-phenylethanol when mutation F176X, responsible for the regioselectivity of the hydroxylation reaction on this substrate, is combined with mutation E103G.

This can be noticed by comparing the data in Fig. 4 and the k_{cat} values in Table 3. The two double mutants with the highest k_{cat} values, (E103G, F176T)- and (E103G, F176I)-ToMO, in fact show high percentages of complexes with very short C-4–C-4 distances and RMSDs, respectively. Mutant (E103G, F176A)-ToMO, the one with the lowest k_{cat} value among the double mutants, is instead predicted to yield only complexes with long C-4–C-4 distances and high RMSDs. The other three double mutants show an intermediate behavior for C-4–C-4 distances and RMSDs and also show intermediate k_{cat} values. We can affirm that the docking procedure that we have developed allows prediction of the relative k_{cat} values of ToMO mutants on the nonphysiological substrate 2-phenylethanol.

Finally, with the aim of investigating a future industrial application of ToMO mutants for the bioconversion of 2-phenylethanol to *p*-tyrosol, we calculated the yield of *p*-tyrosol produced by the most effective catalysts, E103G/F176I and E103G/F176T (Table 3). The yield of *p*-tyrosol produced in a minimal medium by recombinant whole cells was evaluated in batch experiments. *E. coli* strain JM109 cells harboring the plasmid coding for either the E103G/F176I or the E103G/F176T mutant were grown and induced as described in Materials and Methods. After induction, cells were harvested and suspended in M9-G medium containing 2 mM 2-phenylethanol at an OD_{600} of 1. Cells were then incubated at 30°C, under constant shaking at 200 rpm. At different times a 1-ml sample was withdrawn and centrifuged at 12,000 rpm at 4°C for 10 min, and an aliquot of the cell-free supernatant was analyzed by HPLC. The amount of either 2-phenylethanol or *p*-tyrosol was determined by comparing the area of each peak with the area obtained using known concentrations of standards. *p*-Tyrosol was the only isomer produced (within the limits of our assay procedure) with mutants E103G/F176I and E103G/F176T. After 2 h of incubation, the yields of transformation obtained from 2-phenylethanol were 50.2 ± 0.2% for E103G/F176I and 56.3 ± 2.4% for E103G/F176T.

Conclusions. Both directed evolution and rational design approaches have been successfully used in numerous studies probing multicomponent monooxygenase-catalyzed reactions (10, 11, 13, 14, 24, 37, 49, 52). These studies clearly show that these monooxygenases may be considered an archive of powerful and versatile enzymes which can be used to create new catalysts useful for diverse purposes, such as bioremediation of harmful compounds and industrial biosynthesis, among others.

We have previously shown that a fine-tuning of the regioselectivity of the BMM ToMO from *Pseudomonas* sp. OX1 on natural substrates can be achieved through careful alteration of the shape of the active site and that the effects of the mutations on regioselectivity can be quantitatively predicted *a priori* (13, 37). The computational model described in this paper and tested by its application to the synthesis of *p*-tyrosol from 2-phenylethanol, a nonnatural substrate of ToMO, improves the model previously presented for this enzyme (37). Our experimental data validate the computational model presented in this work, showing that mutation of residue F176 allows ToMO to produce exclusively *p*-tyrosol from 2-phenylethanol and that mutation E103G increases the efficiency of catalysis of the enzyme on this substrate.

REFERENCES

1. **Allouche, N., M. Damak, R. Ellouz, and S. Sayadi.** 2004. Use of whole cells of *Pseudomonas aeruginosa* for synthesis of the antioxidant hydroxytyrosol via conversion of tyrosol. Appl. Environ. Microbiol. **70:**2105–2109.
2. **Allouche, N., and S. Sayadi.** 2005. Synthesis of hydroxytyrosol, 2-hydroxyphenylacetic acid, and 3-hydroxyphenylacetic acid by differential conversion of tyrosol isomers using *Serratia marcescens* strain. J. Agric. Food Chem. **53:**6525–6530.
3. **Bailey, L. J., J. G. McCoy, G. N. Phillips, Jr., and B. G. Fox.** 2008. Structural consequences of effector protein complex formation in a diiron hydroxylase. Proc. Natl. Acad. Sci. U. S. A. **105:**19194–19198.
4. **Bertoni, G., F. Bolognese, E. Galli, and P. Barbieri.** 1996. Cloning of the genes for and characterization of the early stages of toluene and o-xylene catabolism in *Pseudomonas stutzeri* OX1. Appl. Environ. Microbiol. **62:**3704–3711.
5. **Bertoni, G., M. Martino, E. Galli, and P. Barbieri.** 1998. Analysis of the gene cluster encoding toluene/o-xylene monooxygenase from *Pseudomonas stutzeri* OX1. Appl. Environ. Microbiol. **64:**3626–3632.
6. **Bouallagui, Z., and S. Sayadi.** 2006. Production of high hydroxytyrosol yields via tyrosol conversion by *Pseudomonas aeruginosa* immobilized resting cells. J. Agric. Food Chem. **54:**9906–9911.
7. **Boyd, D. R., and T. D. Bugg.** 2006. Arene cis-dihydrodiol formation: from biology to application. Org. Biomol. Chem. **4:**181–192.
8. **Boyd, D. R., N. D. Sharma, and C. C. Allen.** 2001. Aromatic dioxygenases: molecular biocatalysis and applications. Curr. Opin. Biotechnol. **12:**564–573.
9. **Bradford, M. M.** 1976. A rapid and sensitive method for the quantitation of microgram quantities of protein utilizing the principle of protein-dye binding. Anal. Biochem. **72:**248–254.
10. **Brouk, M., and A. Fishman.** 2009. Protein engineering of toluene monooxygenases for synthesis of hydroxytyrosol. Food Chem. **116:**114–121.
11. **Brouk, M., Y. Nov, and A. Fishman.** 2010. Improving biocatalyst performance by integrating statistical methods into protein engineering. Appl. Environ. Microbiol. **76:**6397–6403.
12. **Cafaro, V., et al.** 2004. Phenol hydroxylase and toluene/o-xylene monooxygenase from *Pseudomonas stutzeri* OX1: interplay between two enzymes. Appl. Environ. Microbiol. **70:**2211–2219.
13. **Cafaro, V., E. Notomista, P. Capasso, and A. Di Donato.** 2005. Mutation of glutamic acid 103 of toluene o-xylene monooxygenase as a means to control the catabolic efficiency of a recombinant upper pathway for degradation of methylated aromatic compounds. Appl. Environ. Microbiol. **71:**4744–4750.
14. **Cafaro, V., E. Notomista, P. Capasso, and A. Di Donato.** 2005. Regiospecificity of two multicomponent monooxygenases from *Pseudomonas stutzeri* OX1: molecular basis for catabolic adaptation of this microorganism to methylated aromatic compounds. Appl. Environ. Microbiol. **71:**4736–4743.
15. **Cafaro, V., et al.** 2002. Expression and purification of the recombinant subunits of toluene/o-xylene monooxygenase and reconstitution of the active complex. Eur. J. Biochem. **269:**5689–5699.
16. **Capasso, R., et al.** 1995. Antibacterial polyphenols from olive oil mill waste waters. J. Appl. Bacteriol. **79:**393–398.
17. **Covas, M. I., et al.** 2003. Bioavailability of tyrosol, an antioxidant phenolic compound present in wine and olive oil, in humans. Drugs Exp. Clin. Res. **29:**203–206.
18. **Deiana, M., et al.** 1999. Inhibition of peroxynitrite dependent DNA base modification and tyrosine nitration by the extra virgin olive oil-derived antioxidant hydroxytyrosol. Free Radic. Biol. Med. **26:**762–769.
19. **de la Puerta, R., V. Ruiz Gutierrez, and J. R. Hoult.** 1999. Inhibition of leukocyte 5-lipoxygenase by phenolics from virgin olive oil. Biochem. Pharmacol. **57:**445–449.
20. **Dordick, J. S., Y. L. Khmelnitsky, and M. V. Sergeeva.** 1998. The evolution of biotransformation technologies. Curr. Opin. Microbiol. **1:**311–318.
21. **Espin, J. C., C. Soler-Rivas, E. Cantos, F. A. Tomas-Barberan, and H. J. Wichers.** 2001. Synthesis of the antioxidant hydroxytyrosol using tyrosinase as biocatalyst. J. Agric. Food Chem. **49:**1187–1193.
22. **Etschmann, M. M., W. Bluemke, D. Sell, and J. Schrader.** 2002. Biotechnological production of 2-phenylethanol. Appl. Microbiol. Biotechnol. **59:**1–8.
23. **Feingersch, R., J. Shainsky, T. K. Wood, and A. Fishman.** 2008. Protein engineering of toluene monooxygenases for synthesis of chiral sulfoxides. Appl. Environ. Microbiol. **74:**1555–1566.
24. **Fishman, A., Y. Tao, L. Rui, and T. K. Wood.** 2005. Controlling the regio-

specific oxidation of aromatics via active site engineering of toluene para-monooxygenase of *Ralstonia pickettii* PKO1. J. Biol. Chem. **280:**506–514.
25. **Gao, F., and A. J. Daugulis.** 2009. Bioproduction of the aroma compound 2-phenylethanol in a solid-liquid two-phase partitioning bioreactor system by *Kluyveromyces marxianus*. Biotechnol. Bioeng. **104:**332–339.
26. **Ishige, T., K. Honda, and S. Shimizu.** 2005. Whole organism biocatalysis. Curr. Opin. Chem. Biol. **9:**174–180.
27. **Kelsey, N. A., H. M. Wilkins, and D. A. Linseman.** 2010. Nutraceutical antioxidants as novel neuroprotective agents. Molecules **15:**7792–7814.
28. **Laemmli, U. K.** 1970. Cleavage of structural proteins during the assembly of the head of bacteriophage T4. Nature **227:**680–685.
29. **Lazaridis, T., and M. Karplus.** 1999. Discrimination of the native from misfolded protein models with an energy function including implicit solvation. J. Mol. Biol. **288:**477–487.
30. **Lazaridis, T., and M. Karplus.** 1999. Effective energy function for proteins in solution. Proteins **35:**133–152.
31. **Leahy, J. G., P. J. Batchelor, and S. M. Morcomb.** 2003. Evolution of the soluble diiron monooxygenases. FEMS Microbiol. Rev. **27:**449–479.
32. **Lippard, S. J.** 2005. Hydroxylation of C-H bonds at carboxylate-bridged diiron centres. Philos. Trans. A Math. Phys. Eng. Sci. **363:**861–877.
33. **Loughlin, W. A.** 2000. Biotransformations in organic synthesis. Biores. Technol. **74:**49–62.
34. **Manna, C., V. Migliardi, F. Sannino, A. De Martino, and R. Capasso.** 2005. Protective effects of synthetic hydroxytyrosol acetyl derivatives against oxidative stress in human cells. J. Agric. Food Chem. **53:**9602–9607.
35. **Merkx, M., et al.** 2001. Dioxygen activation and methane hydroxylation by soluble methane monooxygenase: a tale of two irons and three proteins. Angew. Chem. Int. ed. Engl. **40:**2782–2807.
36. **Murray, L. J., and S. J. Lippard.** 2007. Substrate trafficking and dioxygen activation in bacterial multicomponent monooxygenases. Acc. Chem. Res. **40:**466–474.
37. **Notomista, E., V. Cafaro, G. Bozza, and A. Di Donato.** 2009. Molecular determinants of the regioselectivity of toluene/o-xylene monooxygenase from *Pseudomonas* sp. strain OX1. Appl. Environ. Microbiol. **75:**823–836.
38. **Notomista, E., A. Lahm, A. Di Donato, and A. Tramontano.** 2003. Evolution of bacterial and archaeal multicomponent monooxygenases. J. Mol. Evol. **56:**435–445.
39. **Owen, R. W., et al.** 2000. Olive-oil consumption and health: the possible role of antioxidants. Lancet Oncol. **1:**107–112.
40. **Parales, R. E., N. C. Bruce, A. Schmid, and L. P. Wackett.** 2002. Biodegradation, biotransformation, and biocatalysis (b3). Appl. Environ. Microbiol. **68:**4699–4709.
41. **Park, J., et al.** 2007. The analysis and application of a recombinant monooxygenase library as a biocatalyst for the Baeyer-Villiger reaction. J. Microbiol. Biotechnol. **17:**1083–1089.
42. **Petroni, A., et al.** 1995. Inhibition of platelet aggregation and eicosanoid production by phenolic components of olive oil. Thromb. Res. **78:**151–160.
43. **Rietjens, S. J., A. Bast, and G. R. Haenen.** 2007. New insights into controversies on the antioxidant potential of the olive oil antioxidant hydroxytyrosol. J. Agric. Food Chem. **55:**7609–7614.
44. **Sambrook, J., E. F. Fritsch, and T. Maniatis.** 1989. Molecular cloning: a laboratory manual, 2nd ed. Cold Spring Harbor Laboratory Press, Cold Spring Harbor, NY.
45. **Sazinsky, M. H., J. Bard, A. Di Donato, and S. J. Lippard.** 2004. Crystal structure of the toluene/o-xylene monooxygenase hydroxylase from *Pseudomonas stutzeri* OX1. Insight into the substrate specificity, substrate channeling, and active site tuning of multicomponent monooxygenases. J. Biol. Chem. **279:**30600–30610.
46. **Sazinsky, M. H., and S. J. Lippard.** 2006. Correlating structure with function in bacterial multicomponent monooxygenases and related diiron proteins. Acc. Chem. Res. **39:**558–566.
47. **Singleton, V. L., R. Orthofer, and R. M. Lamuela-Raventós.** 1999. Analysis of total phenols and other oxidation substrates and antioxidants by means of Folin-Ciocalteu reagent. Methods Enzymol. **299:**152–178.
48. **Straathof, A. J., S. Panke, and A. Schmid.** 2002. The production of fine chemicals by biotransformations. Curr. Opin. Biotechnol. **13:**548–556.
49. **Tao, Y., A. Fishman, W. E. Bentley, and T. K. Wood.** 2004. Altering toluene 4-monooxygenase by active-site engineering for the synthesis of 3-methoxycatechol, methoxyhydroquinone, and methylhydroquinone. J. Bacteriol. **186:**4705–4713.
50. **Torres Pazmino, D. E., M. Winkler, A. Glieder, and M. W. Fraaije.** 2010. Monooxygenases as biocatalysts: classification, mechanistic aspects and biotechnological applications. J. Biotechnol. **146:**9–24.
51. **Vardar, G., Y. Tao, J. Lee, and T. K. Wood.** 2005. Alanine 101 and alanine 110 of the alpha subunit of *Pseudomonas stutzeri* OX1 toluene-o-xylene monooxygenase influence the regiospecific oxidation of aromatics. Biotechnol. Bioeng. **92:**652–658.
52. **Vardar, G., and T. K. Wood.** 2005. Protein engineering of toluene-o-xylene monooxygenase from *Pseudomonas stutzeri* OX1 for enhanced chlorinated ethene degradation and o-xylene oxidation. Appl. Microbiol. Biotechnol. **68:**510–517.
53. **Viggiani, A., et al.** 2004. The role of the conserved residues His-246, His-199, and Tyr-255 in the catalysis of catechol 2,3-dioxygenase from *Pseudomonas stutzeri* OX1. J. Biol. Chem. **279:**48630–48639.
54. **Visioli, F., A. Poli, and C. Gall.** 2002. Antioxidant and other biological activities of phenols from olives and olive oil. Med. Res. Rev. **22:**65–75.
55. **Watanabe, K., H. Futamata, and S. Harayama.** 2002. Understanding the diversity in catabolic potential of microorganisms for the development of bioremediation strategies. Antonie Van Leeuwenhoek **81:**655–663.
56. **Waterman, E., and B. Lockwood.** 2007. Active components and clinical applications of olive oil. Altern. Med. Rev. **12:**331–342.